JACS
JOURNAL OF THE AMERICAN CHEMICAL SOCIETY

Communication

pubs.acs.org/JACS

N-Alkyldinaphthocarbazoles, Azaheptacenes, for Solution-Processed Organic Field-Effect Transistors

Toan V. Pho,[†,‡] Jonathan D. Yuen,[‡] Joshua A. Kurzman,[†] Braden G. Smith,[†] Maosheng Miao,[§] Wesley T. Walker,[∥] Ram Seshadri,[†,§] and Fred Wudl*[,†,‡,§]

[†]Department of Chemistry and Biochemistry, [‡]Center for Polymers and Organic Solids, and [§]Department of Materials and Materials Research Laboratory, University of California, Santa Barbara, California 93106, United States

[∥]Department of Chemistry and Biochemistry, University of California, Los Angeles, California 90095, United States

Supporting Information

ABSTRACT: Substituted *N*-alkyldinaphthocarbazoles were synthesized using a key double Diels–Alder reaction. The angular nature of the dinaphthocarbazole system allows for increased stability of the conjugated system relative to linear analogues. The *N*-alkyldinaphthocarbazoles were characterized by UV–vis absorption and fluorescence spectroscopy as well as cyclic voltammetry. X-ray structure analysis based on synchrotron X-ray powder diffraction revealed that the *N*-dodecyl-substituted compound was oriented in an intimate herringbone packing motif, which allowed for p-type mobilities of 0.055 $cm^2\ V^{-1}\ s^{-1}$ from solution-processed organic field-effect transistors.

Since the advent of the organic field-effect transistor (OFET), linear polyacenes and their derivatives have emerged as promising materials for small-molecule hole-transporting OFETs.[1−3] In particular, tetracene and pentacene have been extensively studied because the combination of their delocalized π systems and solid-state structure/morphology provide them with high charge-carrier mobilities. The more extended acenes, such as hexacene and heptacene, may demonstrate enhanced transport properties due to their increased π conjugation, but these acenes have been underutilized, primarily because of the instability of their π systems as well as processing difficulties arising from the insolubility of the unfunctionalized systems.[1]

Whereas unsubstituted extended acenes (i.e., hexacene through nonacene) are stable in a polymeric matrix for only a few hours,[4−6] stable and soluble extended acene derivatives have been prepared via extensive functionalization of the acene core to provide both steric and electronic protection.[7−12] The stability of extended polyacenes can also be improved by disrupting the linearity of the catacondensed array, thus decreasing their proclivity toward dimerization and polymerization. This is best exemplified by the increased stability of the angular "phenes" relative to their isomeric linear acene counterparts.[13,14] In addition, the shift from a linear acene to its angular analogue is typically accompanied by a stabilization of the highest occupied molecular orbital (HOMO) level,[15] thereby mitigating the oxidative degradation processes that plague the linear polyacenes.

Similarly, the introduction of heteroatoms such as sulfur or nitrogen[16−22] into the polyacene backbone allows for added stability arising from the loss of linearity of the fused system. The inclusion of these heterocycles also provides sites where solubilizing groups or additional functional motifs can readily be appended. For these reasons, we studied the chemical and electronic properties of one of the simplest heteroheptacenes, dinaphthocarbazole (DNC), which is composed of a carbazole ring laterally fused to two naphthalene substituents.

First reported in 1962,[23] unfunctionalized DNC was synthesized by Elbs pyrolysis of a bis(*o*-tolyl)ketone precursor. However, the low yield (ca. 0.5% for the key pyrolysis step) and insolubility of the target DNC have precluded its application in organic electronics. Herein we report the synthesis of soluble substituted DNCs in moderate yields via a double Diels–Alder reaction[24] and our evaluation of their performance in p-type OFETs.

The synthesis of the substituted DNCs (Scheme 1) was adapted from a synthetic procedure for tetrasubstituted carbazoles.[24] Thermolysis of diacetate **1**[24] provided a transient diene that underwent a double Diels–Alder reaction with 2 equiv of 1,4-naphthoquinone to give octahydrocarbazole **2**.

Scheme 1. Synthesis of DNCs[a]

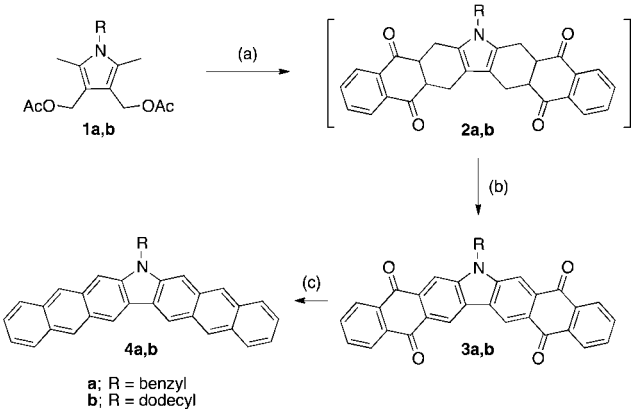

[a]Conditions: (a) 1,4-naphthoquinone, mesitylene, reflux; (b) reflux; (c) Al, $HgCl_2$, CBr_4, cyclohexanol, reflux.

Received: August 20, 2012
Published: October 17, 2012

   dx.doi.org/10.1021/ja3082582 | *J. Am. Chem. Soc.* 2012, 134, 18185−18188

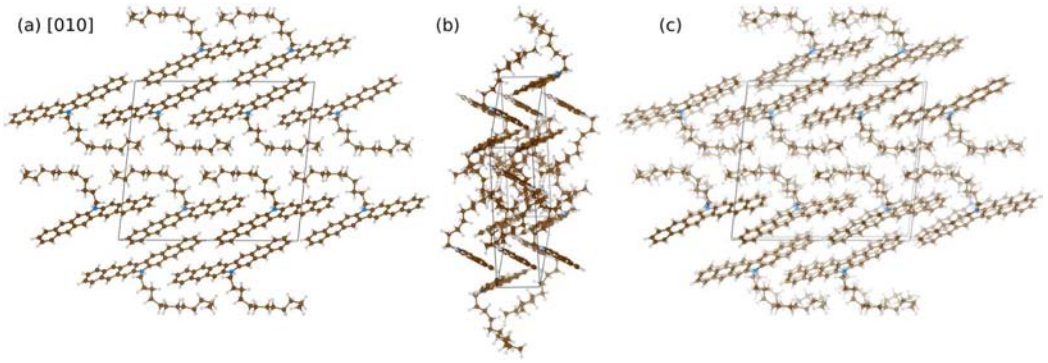

Figure 1. (a) X-ray crystal structure projected down the *b* axis and (b) herringbone packing motif of DNC **4b**. (c) DFT-optimized crystal structure of **4b** overlaid on the structure determined using powder diffraction.

Whereas the literature protocol required an oxidizing agent such as 2,3-dichloro-5,6-dicyanobenzoquinone (DDQ) to aromatize the octahydrocarbazole, we found that excess naphthoquinone could be used in the one-pot reaction to oxidize **2** to the corresponding bisanthraquinone **3**. Reduction mediated by aluminum amalgam then afforded the substituted DNC **4**. Despite the modest yields (40−45%) of the bis-cycloaddition, this synthesis provides a versatile pathway to various substituted DNCs. The *N*-benzyl derivative **4a** was synthesized first, but its low solubility provided an impetus for the synthesis of the significantly more soluble *N*-dodecyl analogue **4b**.

Because attempts to produce crystals of the DNCs suitable for single-crystal X-ray diffraction were unsuccessful, the X-ray crystal structure of DNC **4b** was instead modeled from synchrotron X-ray powder diffraction data. The crystal structure model was obtained using the parallel tempering algorithm of the Monte Carlo-simulated annealing method implemented in FOX.[25] The input molecular structure was optimized within the framework of density functional theory (DFT) using Gaussian 03.[26] The 6-31G(d) basis set was used, and the exchange−correlation potential and energy were described using the B3LYP hybrid functional. In the structure optimization simulation, the molecules were allowed to translate and rotate around the center of mass and their dihedral angles were allowed to change, subject to the constraints imposed by the unit cell dimensions and space group symmetry. The ring system was constrained as a rigid body, leaving the dodecyl chain bound through the carbazole nitrogen as the only fragment in which the torsion angles and bond distances were allowed to vary. Soft restraints were applied to the bond distances in the alkyl chain. Because of the large number of atoms in the asymmetric unit and the modest crystallinity of the sample, attempts to refine the atom positions were unsuccessful. Thus, the model presented in Figure 1 was obtained directly from the Monte Carlo simulation without further optimization. Nonetheless, the visual agreement between the observed and calculated diffraction intensities is impressive [Figure S1 in the Supporting Information (SI)], and the statistical figures of merit [χ^2 (GoF) = 3.8; R_{wp} = 11.7%; R_p = 7.5%] also support the plausibility of the proposed model.

To assess the validity of the model further, the crystal structure was also optimized by periodic DFT within the generalized gradient approximation (GGA) of Perdew, Burke, and Ernzerhof (PBE) using VASP.[27] In Figure 1c, the DFT-optimized crystal structure of DNC **4b** is overlaid on the structure determined using powder diffraction. Additional details regarding the diffraction and DFT methods are available in the SI. Despite the tendency of the PBE functional to overestimate lattice constants and bond distances, the DFT-optimized unit cell volume was less than that determined experimentally, suggesting that there may have been some residual solvent trapped in the sample. This is consistent with the fact that the measured density of the sample (1.20 g/cm^3) was slightly larger than the density calculated from the crystal structure (1.16 g/cm^3).

According to Figure 1a, the fused rings of DNC **4b** adopt an angular configuration due to the central pyrrole unit. The strong hydrophobic interaction between the dodecyl side chains promotes segregation of the alkyl groups and the aromatic cores within the unit cell. Moreover, the closest face-to-face distance between the π systems is the *b*-axis cell constant (5.84 Å), which is too large for intermolecular $\pi-\pi$ stacking. However, the molecules are oriented in an intimate herringbone packing motif (Figure 1b) in which the closest C−C distance is 3.78 Å, auguring well for facile intermolecular charge transport.

UV−vis absorption studies of the DNCs (Figure 2a) revealed absorption onsets at ca. 570 nm, with the N-substitution exerting a negligible influence on the photophysical properties. Although the DNCs are colored red, the actual absorption in

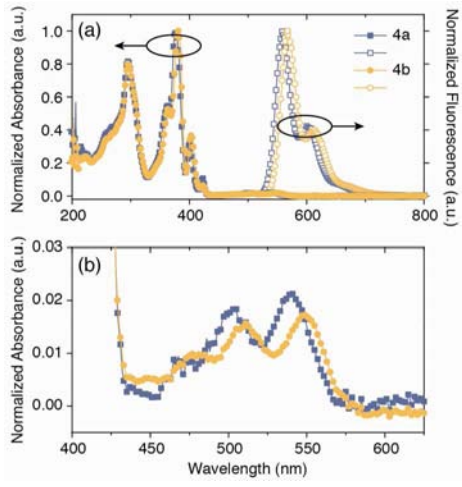

Figure 2. (a) UV−vis absorption (● and ■) and fluorescence (○ and □) spectra of the DNCs in chloroform. (b) Magnified (higher-gain) view of the absorption spectrum in the 400−550 nm region, showing the typical acene "fingerlike" absorption.

dx.doi.org/10.1021/ja3082582 | J. Am. Chem. Soc. 2012, 134, 18185−18188

the visible region from 450 to 570 nm is quite minimal (Figure 2b). Strong vibronic structure was observed throughout the UV−vis spectrum, which is typical of similar aromatic hydrocarbons.[28] The UV−vis spectra of the DNCs underwent a slight bathochromic shift (ca. 30 nm) relative to the absorption profile of their angular arene analogue, heptaphene.[29] This red shift is most likely due to the electron-donating character of the nitrogen atom. The DNCs also displayed a yellow-orange fluorescence in organic solvents such as toluene and chloroform (λ_{max} = 559 and 570 nm for **4a** and **4b**, respectively, in chloroform with an excitation wavelength of 510 nm). The fluorescence quantum yields of the *N*-benzyl and *N*-dodecyl derivatives in chloroform were determined to be 30 and 25%, respectively, relative to a standard of rhodamine B in ethanol.

The electrochemical properties of the DNCs were studied by cyclic voltammetry (CV) (Table S1 in the SI). The DNCs exhibited a reversible oxidation wave (Figure S2), whereas no reduction behavior was observed. The HOMO level of −5.0 eV suggests that the DNCs should be relatively air-stable, supporting the empirical observations of air stability.

The atomic and electronic structures of isolated DNC molecules were probed by DFT calculations at the B3LYP/6-31G(d) level as implemented in Gaussian 03 (Figure S3). The HOMOs and LUMOs of DNCs **4a** and **4b** were computed to be completely delocalized over the entire dinaphthocarbazole core, and the HOMO and LUMO energies of **4b** were calculated to be −4.7 and −1.9 eV, respectively. The calculated HOMO level is 0.3 eV higher than the experimental value, whereas the LUMO level is 1 eV higher than the value of −2.9 eV estimated from the experimental HOMO level and the optical gap. The calculated gap therefore is 0.7 eV greater than that obtained from the optical measurements; this discrepancy is likely caused by neglect of the exciton effect, which may be quite severe for this molecule since the HOMO and LUMO orbitals overlap significantly. Time-dependent DFT (TD-DFT) calculations at the B3LYP/6-31G(d) level on an *N*-methyl-substituted DNC subsequently provided a theoretical band gap of 2.38 eV, which is significantly closer to the experimental band gap of 2.1 eV.

Thermogravimetric analysis (TGA) revealed that both DNCs exhibited good thermal stability, with 5 wt % loss occurring at ca. 370 °C (Table S1 and Figure S4). Differential scanning calorimetry (DSC) showed that benzyl-substituted DNC **4a** decomposed without melting, whereas dodecyl-substituted DNC **4b** melted at 235 °C.

Because of its improved solubility relative to the benzyl derivative **4a**, dodecyl-substituted DNC **4b** was chosen for use in solution-processed OFETs. Bottom-gate, Au bottom-contact OFETs were fabricated on heavily doped n-type Si wafers with a thermally grown 200 nm thick SiO_2 layer. A chloroform solution of **4b** (10 mg mL^{-1}) was then spin-cast onto the decyltrichlorosilane (DTS)-treated SiO_2 substrates. A more detailed description of the fabrication process is provided in the SI. Annealing the devices at temperatures ranging from 80 to 200 °C resulted in small changes in the charge-carrier mobility, and the highest average mobility (0.055 cm^2 V^{-1} s^{-1}) was achieved at an annealing temperature of 160 °C. The transfer and output curves of the device annealed at 160 °C are shown in Figure 3. The mobility was somewhat lower than those of other (particularly spin-cast) seven-ring organic semiconductors,[30,31] which may be attributed to the lack of intermolecular HOMO overlap between neighboring heteroatoms, as orbital overlap between heteroatoms has been shown to enhance the mobility of heteroacenes.[32] DFT calculations of two neighboring DNC molecules from the crystal structure revealed that the HOMO extends onto only the anthracene portion of the nearest neighbor (Figure S5). Finally, given that solution-processed small molecules tend to exhibit lower charge-carrier mobilities because of the presence of numerous grain boundaries, we expect that vacuum-processed devices may exhibit better performance due to their larger crystalline domains and the resulting more facile charge transport. Further investigations to optimize the charge-carrier mobility are in progress.

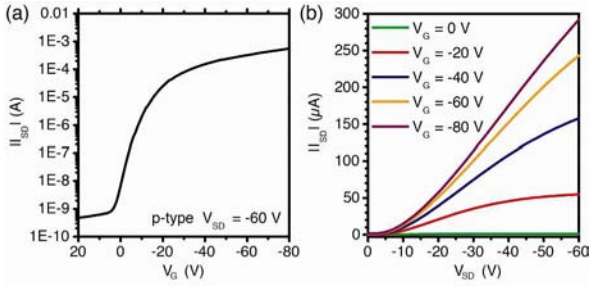

Figure 3. (a) Transfer and (b) output curves in p-type operation mode of the OFETs using DNC **4b**.

In summary, substituted DNCs have been synthesized and utilized in solution-processed OFETs. The enhanced stability of the DNCs relative to linear heptacene derivatives allows for the study of the charge transport characteristics of these angular heteroheptacenes. Hole mobilites of 0.055 cm^2 V^{-1} s^{-1} were obtained, and additional studies to determine the optimal morphology and long-range ordering for increased charge-carrier mobility are currently underway.

■ ASSOCIATED CONTENT

Supporting Information

Synthetic details, CV data, molecular orbital diagrams, X-ray structure determination, device fabrication details, crystallographic data (CIF), and complete ref 26. This material is available free of charge via the Internet at http://pubs.acs.org.

■ AUTHOR INFORMATION

Corresponding Author

wudl@chem.ucsb.edu

Notes

The authors declare no competing financial interest.

■ ACKNOWLEDGMENTS

T.V.P., J.A.K., B.G.S., M.M., R.S., and F.W. acknowledge support from the ConvEne IGERT Program (NSF-DGE 0801627). Use of the Advanced Photon Source at Argonne National Laboratory was supported by the U.S. Department of Energy, Office of Science, Office of Basic Energy Sciences, under Contract DE-AC02-06CH11357. We acknowledge support from the Center for Scientific Computing at the California NanoSystems Institute and the MRL, funded by NSF MRSEC (DMR-1121053) and NSF CNS-0960316. J.A.K. acknowledges partial support from the IMI Program of the National Science Foundation under Award DMR-0843934 and thanks Jean-Nöel Chotard for guidance in using FOX.

REFERENCES

(1) Bendikov, M.; Wudl, F.; Perepichka, D. F. *Chem. Rev.* **2004**, *104*, 4891.
(2) Anthony, J. E. *Angew. Chem., Int. Ed.* **2008**, *47*, 452.
(3) Anthony, J. E. *Chem. Rev.* **2006**, *106*, 5028.
(4) Mondal, R.; Adhikari, R. M.; Shah, B. K.; Neckers, D. C. *Org. Lett.* **2007**, *9*, 2505.
(5) Mondal, R.; Shah, B. K.; Neckers, D. C. *J. Am. Chem. Soc.* **2006**, *128*, 9612.
(6) Tönshoff, C.; Bettinger, H. F. *Angew. Chem., Int. Ed.* **2010**, *49*, 4125.
(7) Chun, D.; Cheng, Y.; Wudl, F. *Angew. Chem., Int. Ed.* **2008**, *47*, 8380.
(8) Kaur, I.; Jazdzyk, M.; Stein, N. N.; Prusevich, P.; Miller, G. P. *J. Am. Chem. Soc.* **2010**, *132*, 1261.
(9) Payne, M. M.; Parkin, S. R.; Anthony, J. E. *J. Am. Chem. Soc.* **2005**, *127*, 8028.
(10) Kaur, I.; Stein, N. N.; Kopreski, R. P.; Miller, G. P. *J. Am. Chem. Soc.* **2009**, *131*, 3424.
(11) Zade, S. S.; Bendikov, M. *Angew. Chem., Int. Ed.* **2010**, *49*, 4012.
(12) Purushothaman, B.; Parkin, S. R.; Anthony, J. E. *Org. Lett.* **2010**, *12*, 2060.
(13) Clar, E. *Polycyclic Hydrocarbons*; Academic Press: London, 1964.
(14) Harvey, R. G. *Polycyclic Aromatic Hydrocarbons: Chemistry and Carcinogenicity*; Cambridge University Press: Cambridge, U.K., 1991.
(15) Wiberg, K. B. *J. Org. Chem.* **1997**, *62*, 5720.
(16) Gao, P.; Cho, D.; Yang, X.; Enkelmann, V.; Baumgarten, M.; Müllen, K. *Chem.—Eur. J.* **2010**, *16*, 5119.
(17) Zheng, Q.; Chen, S.; Zhang, B.; Wang, L.; Tang, C.; Katz, H. E. *Org. Lett.* **2011**, *13*, 324.
(18) Sirringhaus, H.; Friend, R. H.; Wang, C.; Leuninger, J.; Müllen, K. *J. Mater. Chem.* **1999**, *9*, 2095.
(19) Bouchard, J.; Wakim, S.; Leclerc, M. *J. Org. Chem.* **2004**, *69*, 5705.
(20) Wakim, S.; Bouchard, J.; Blouin, N.; Michaud, A.; Leclerc, M. *Org. Lett.* **2004**, *6*, 3413.
(21) Wex, B.; Kaafarani, B. R.; Schroeder, R.; Majewski, L. A.; Burckel, P.; Grell, M.; Neckers, D. C. *J. Mater. Chem.* **2006**, *16*, 1121.
(22) Yamamoto, T.; Takimiya, K. *J. Am. Chem. Soc.* **2007**, *129*, 2224.
(23) Zander, M.; Franke, W. *Chem. Ber.* **1963**, *96*, 699.
(24) Vessels, J. T.; Janicki, S. Z.; Petillo, P. A. *Org. Lett.* **2000**, *2*, 73.
(25) Favre-Nicolin, V.; Cerny, R. *J. Appl. Crystallogr.* **2002**, *35*, 734.
(26) Frisch, M. J.; et al. *Gaussian 03*, revision D.01; Gaussian, Inc.: Wallingford, CT, 2004.
(27) Kresse, G.; Furthmüller, J. *Phys. Rev. B* **1996**, *54*, 11169.
(28) Malkin, J. *Photophysical and Photochemical Properties of Aromatic Compounds*; CRC Press: Boca Raton, FL, 1992.
(29) Clar, E.; Kelly, W. *J. Am. Chem. Soc.* **1954**, *76*, 3502.
(30) Goetz, K. P.; Li, Z.; Ward, J. W.; Bougher, C.; Rivnay, J.; Smith, J.; Conrad, B. R.; Parkin, S. R.; Anthopoulos, T. D.; Salleo, A.; Anthony, J. E.; Jurchescu, O. D. *Adv. Mater.* **2011**, *23*, 3698.
(31) Hoppe, A.; Seekamp, J.; Balster, T.; Gotz, G.; Bauerle, P.; Wagner, V. *Appl. Phys. Lett.* **2007**, *91*, No. 132115.
(32) Takimiya, K.; Shinamura, S.; Osaka, I.; Miyazaki, E. *Adv. Mater.* **2011**, *23*, 4347.